2013

On the detectability of eccentric binary pulsars

Manjari Bagchi

Duncan R. Lorimer

Spencer Wolfe

Mon. Not. R. Astron. Soc. **000**, 000–000 (0000) Printed 13 August 2018 (MN LATEX style file v2.2)

On the detectability of eccentric binary pulsars

Manjari Bagchi[1⋆], Duncan R. Lorimer[1,2,3] and Spencer Wolfe[1]

[1] *Department of Physics, White Hall, West Virginia University, Morgantown, WV 26506, USA*
[2] *NRAO, Green Bank Observatory, PO Box 2, Green Bank, WV 24944, USA*
[3] *Astrophysics, University of Oxford, Denys Wilkinson Building, Keble Road, Oxford OX1 3RH*

13 August 2018

ABSTRACT

By generalizing earlier work of Johnston & Kulkarni, we present a detailed description of the reduction in the signal-to-noise ratio for observations of binary pulsars. We present analytical expressions, and provide software, to calculate the sensitivity reduction for orbits of arbitrary eccentricity. We find that this reduction can be quite significant, especially in the case of a massive companion like another neutron star or a black hole. On the other hand, the reduction is less for highly eccentric orbits. We also demonstrate that this loss of sensitivity can be recovered by employing "acceleration search" or "acceleration-jerk search" algorithms.

Key words: stars: neutron — pulsars: general — methods: analytical – methods: numerical

1 INTRODUCTION

It is now well established that studies of binary pulsar systems provide a unique means to test relativistic theories of gravity in the strong-field regime (Stairs 2005; Kramer & Stairs 2008), with the most stringent tests often possible in systems with short orbital periods and high eccentricities. Detecting such systems in pulsar searches is challenging due to the Doppler modulation of the pulsed signal as the pulsar moves with respect to the centre of mass of the binary system during an observation. In an earlier study, Johnston & Kulkarni (1991; hereafter JK91) derived an analytical framework to compute the reduction of the signal-to-noise ratio due to binary motion for the case of circular orbits. This work also considered the improvement in sensitivity due to "acceleration searches" in which the data are corrected for binary motion either in the time (Anderson 1993) or frequency domain (Ransom 2001).

Although circular orbits are applicable to many known binary pulsar systems (Lorimer 2008), for the purposes of a growing number of studies, it is desirable to compute the loss of sensitivity in eccentric binary systems for different types of companions. The purpose of this paper is to extend the work of JK91 to consider the case of orbits with arbitrary eccentricity. This framework allows us to compute the sensitivity degradation for any type of binary system, therefore allowing detailed investigation of survey sensitivity limits, which is applicable to a number of statistical studies (see Ridley & Lorimer (2010) for example). While Ramachandran & Portegies Zwart (1998) investigated this, they did not provide explicit analytical expressions, nor did they extensively explore the parameter space implied by pulsar surveys and the different types of binary systems. We will discuss more about their work later when appropriate.

The plan for the rest of this paper is as follows. The analytical expressions to describe this problem are developed in Section 2, numerical methods to employ those expressions are elaborated in Section 3, and some applications of the model in different cases are reported in Section 4. Finally, our conclusions are given in Section 5.

⋆ Email: Manjari.Bagchi@mail.wvu.edu

2 FORMULATION

Following JK91, we consider a pulsar with spin period P_p. The signal emitted from the pulsar at an arbitrary time t can be written as a summation of Fourier components:

$$S_p(t) = \sum_{k=1}^{k=\infty} a_k \exp\left(ik\omega_p t + i\psi_k\right), \tag{1}$$

where $\omega_p = 2\pi/P_p$ is the angular spin frequency of the pulsar, ψ_k is the phase factor of the $k^{\rm th}$ component and $i = \sqrt{-1}$. The signal received on the Earth

$$S_R(t) = \sum_{k=1}^{k=\infty} a_k \exp\left(ik\omega_p \left(t + \frac{d}{c}\right) + i\psi_k\right), \tag{2}$$

where d is the distance between the pulsar and the Earth at time t and c is the speed of light. The $m^{\rm th}$ harmonic of the received signal is

$$S_R^m(t) = a_m \exp\left(im\omega_p \left(t + \frac{d}{c}\right) + i\psi_m\right). \tag{3}$$

Using a Taylor series expansion of d, we can write the distance to the pulsar

$$d = d_0 + v_{l0}t + \frac{a_{l0}t^2}{2!} + \frac{j_{l0}t^3}{3!} + \ldots, \tag{4}$$

where v_l is the line-of-sight velocity, a_l is the line-of-sight acceleration, and j_l is the line-of-sight jerk at the time t; v_{l0}, a_{l0} and j_{l0} are the values of these quantities at $t = 0$. d_0 is the distance between the pulsar and the Earth at $t = 0$. An isolated pulsar moves with a constant velocity, so a_l, j_l (and higher order terms) are zero; but, this is not the case for a binary pulsar. Similarly, for v_l, the Taylor series expansion gives

$$v_l = v_{l0} + a_{l0}t + \frac{j_{l0}t^2}{2!} + \ldots \tag{5}$$

Integrating this expression with respect to time, we get

$$\int_0^t v_l\, dt = \int_0^t \left(v_{l0} + a_{l0}t + \frac{j_{l0}t^2}{2!} + \ldots\right) dt = v_{l0}t + \frac{a_{l0}t^2}{2!} + \frac{j_{l0}t^3}{3!} + \ldots \tag{6}$$

So Equation (4) becomes

$$d = d_0 + \int_0^t v_l\, dt. \tag{7}$$

To detect a pulsar, one performs a Fourier transform of the time series of the received signal as $\mathcal{F}\left[S_R(t)\right] = \int_0^T S_R(t)\exp(-i\omega t)\, dt$ which gives the power as $\left|\mathcal{F}\left[S_R(t)\right]\right|^2$. Here T is the duration of the observation. Because the signal has a small duty cycle instead of being purely sinusoidal, several harmonics are present in the Fourier power spectrum. One usually performs "harmonic summing" up to the $n^{\rm th}$ harmonic to increase the search sensitivity by a factor of up to $\sqrt{n}$ (see, e.g., Lorimer & Kramer 2005). From Equation (3), the power of the $m^{\rm th}$ harmonic in the Fourier spectrum can be written as

$$\begin{aligned}
\left|\mathcal{F}\left[S_R^m(t)\right]\right|^2 &= \left|\int_0^T a_m \exp\left(im\omega_p\left(t + \frac{d}{c}\right) + i\psi_m\right)\exp(-i\omega t)\, dt\right|^2 \\
&= \left|\int_0^T a_m \exp\left(im\omega_p\left(t + \frac{1}{c}\left(d_0 + v_{l0}t + \frac{a_{l0}t^2}{2!} + \frac{j_{l0}t^3}{3!} + \ldots\right)\right) + i\psi_m\right)\exp(-i\omega t)\, dt\right|^2 \\
&= \left|\int_0^T a_m \exp\left(\frac{im\omega_p d_0}{c} + i\psi_m\right)\exp\left(\frac{im\omega_p}{c}\left[(1 + \frac{v_{l0}}{c})ct + \frac{a_{l0}t^2}{2!} + \frac{j_{l0}t^3}{3!} + \ldots\right]\right)\exp(-i\omega t)\, dt\right|^2,
\end{aligned} \tag{8}$$

where we note that d_0 contributes only as a constant phase factor and

$$m\,\omega_p^{'} = m\,\omega_p\left[(1 + \frac{v_{l0}}{c}) + \frac{a_{l0}t}{c\,2!} + \frac{j_{l0}t^2}{c\,3!} + \ldots\right] \tag{9}$$

is the observed angular spin frequency of the $m^{\rm th}$ harmonic. As $m\,\omega_p^{'}$ changes with t, the power gets distributed over adjacent Fourier bins leading to a loss in sensitivity. Nevertheless, the pulsar can be detected in the Fourier bin where the power is maximum. In the case of a pulsar moving with a constant velocity, the power of the $m^{\rm th}$ harmonic will be peaked at the Fourier bin of angular frequency $m\,\omega_p\,(1 + \frac{v_{l0}}{c})$ which is the conventional Doppler effect.

Following JK91 let us define three efficiency factors, γ_{1m}, γ_{2m} and γ_{3m}. The factor γ_{1m}^2 is the ratio of the height of the power of the $m^{\rm th}$ harmonic in the Fourier spectrum when the acceleration, jerk, and other higher order derivatives of the pulsar are non-zero, to the height when these terms are zero, *i.e.*, the pulsar has a constant velocity. This can be written as follows

$$\gamma_{1m}(\alpha_v, T) = \frac{1}{T}\left|\int_0^T \exp\left[\frac{im\omega_p}{c}\left(v_{l0}t + \frac{a_{l0}t^2}{2!} + \frac{j_{l0}t^3}{3!} + \ldots - \alpha_v t\right)\right] dt\right| = \frac{1}{T}\left|\int_0^T \exp\left[\frac{im\omega_p}{c}\left(\left(\int_0^t v_l\, dt\right) - \alpha_v t\right)\right] dt\right|, \tag{10}$$

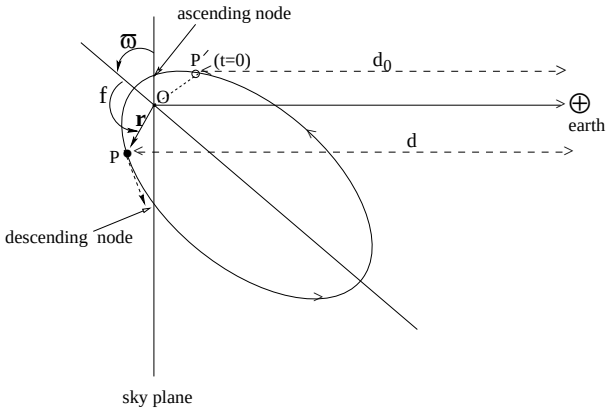

Figure 1. The orbit of a pulsar in a binary system, projected onto a plane containing the line of sight, *i.e.*, perpendicular to the sky plane. The semi-major axis of the projected ellipse $a_p^{'} = a_p \sin i$ where i is the orbital inclination angle and a_p is the semi-major axis of the actual orbit of the pulsar. $P^{'}$ is the location of the pulsar at $t = 0$ and P is the location of the pulsar at any arbitrary time t. f is the true anomaly and ϖ is the longitude of the periastron. d_0 is the distance between the pulsar and the Earth at $t = 0$ and d is the distance between the pulsar and the Earth at t.

where α_v is a free parameter. The pulsar will be detected for such a value of α_v which maximizes γ_{1m} with apparent frequency of the $m^{\rm th}$ harmonic as $m\omega_p^{'} = m\omega_p\,(1 + \alpha_v/c)$. Clearly, the maximum value of $\gamma_{1m}^2 = 1$ is possible only when the pulsar moves with a constant velocity, giving $\alpha_v = v_{l0}$.

The above efficiency factor γ_{1m} essentially describes the sensitivity loss of a standard pulsar search. Acceleration searches attempt to improve upon this efficiency by accounting for the Doppler shifting of the pulsar signal during the observation. A review of some of the various techniques that have been developed so far can be found in Lorimer & Kramer (2005). The most common type of acceleration search assumes that the line-of-sight acceleration during the observation is a constant value. This is a good approximation for binary periods that are significantly longer than the survey integration time, and we consider these searches using the efficiency factor γ_{2m}. Specifically, γ_{2m}^2 is the ratio of the height of the power of the $m^{\rm th}$ harmonic in the Fourier spectrum when the jerk and other higher order derivatives of the pulsar are non-zero, to the height when these terms are zero, *i.e.*, the pulsar has a constant acceleration. Expressing this idea mathematically, we have

$$\begin{aligned}\gamma_{2m}(\alpha_a, \alpha_v, T) &= \frac{1}{T}\Big|\int_0^T \exp\left[\frac{im\omega_p}{c}\left(v_{l0}t + \frac{a_{l0}t^2}{2!} + \frac{j_{l0}t^3}{3!} + \ldots - \alpha_a t^2 - \alpha_v t\right)\right] dt\Big| \\ &= \frac{1}{T}\Big|\int_0^T \exp\left[\frac{im\omega_p}{c}\left(\left(\int_0^t v_l\, dt\right) - \alpha_a t^2 - \alpha_v t\right)\right] dt\Big|, \end{aligned} \tag{11}$$

where α_a, α_v are free parameters. The use of an acceleration search algorithm leads to the detection of the pulsar for such a set of values of α_a and α_v which maximizes γ_{2m}. Clearly, the maximum value of $\gamma_{2m}^2 = 1$ is possible only when the pulsar moves with a constant acceleration, giving $\alpha_v = v_{l0}$ and $\alpha_a = a_{l0}/2!$.

Due to the additional computational requirements, searches involving the unknown jerk term are less commonly carried out. To investigate their relative efficiency, however, we define γ_{3m} such that γ_{3m}^2 is the ratio of the height of the power of the $m^{\rm th}$ harmonic in the Fourier spectrum when the derivative of the jerk and other higher order derivatives of the pulsar are non-zero, to the height when these terms are zero, *i.e.*, the pulsar has a constant jerk. With this in mind, we may write

$$\begin{aligned}\gamma_{3m}(\alpha_j, \alpha_a, \alpha_v, T) &= \frac{1}{T}\Big|\int_0^T \exp\left[\frac{im\omega_p}{c}\left(v_{l0}t + \frac{a_{l0}t^2}{2!} + \frac{j_{l0}t^3}{3!} + \ldots - \alpha_j t^3 - \alpha_a t^2 - \alpha_v t\right)\right] dt\Big| \\ &= \frac{1}{T}\Big|\int_0^T \exp\left[\frac{im\omega_p}{c}\left(\left(\int_0^t v_l\, dt\right) - \alpha_j t^3 - \alpha_a t^2 - \alpha_v t\right)\right] dt\Big|, \end{aligned} \tag{12}$$

where α_j, α_a, and α_v are free parameters. Such a search process would detect a pulsar with a set of values of α_j, α_a and α_v which maximizes γ_{3m}. Clearly, the maximum value of $\gamma_{3m}^2 = 1$ is possible only when the pulsar moves with a constant jerk, giving $\alpha_v = v_{l0}$, $\alpha_a = a_{l0}/2!$ and $\alpha_j = j_{l0}/3!$.

To compute the relevant line-of-sight terms in the above expressions, we need to consider the shape of the pulsar orbit. We denote the semi-major axis of the pulsar orbit to be a_p and the semi-major axis of the ellipse projected perpendicular to the plane of the sky to be $a_p^{'} = a_p \sin i$ where i is the orbital inclination angle. This projected ellipse is shown in Fig. 1 where f is the true anomaly and ϖ is the longitude of the periastron. The pulsar is located at $P^{'}$ at $t = 0$ and at P at an arbitrary time t. If $\mathbf{r}$ is the radius vector of the position of the pulsar at t with magnitude r, then the projection of r along the line of sight is given by

$$r_l = r \sin\,(f + \varpi). \tag{13}$$

Similarly, the projection of the magnitude r_0 of the radius vector of the pulsar at $t = 0$ can be written as

$$r_{l0} = r_0 \sin(f_0 + \varpi), \tag{14}$$

where f_0 is the true anomaly at $t = 0$. We can write

$$\int_0^t v_l \, dt = (r_l - r_{l0}). \tag{15}$$

So, Equation (7) becomes

$$d = d_0 + (r_l - r_{l0}). \tag{16}$$

Using Equation (15), Equations (10), (11) and (12) become

$$\gamma_{1m}(\alpha_v, T) = \frac{1}{T}\left|\int_0^T \exp\left[\frac{im\omega_p}{c}(r_l - r_{l0} - \alpha_v t)\right] dt\right|, \tag{17}$$

$$\gamma_{2m}(\alpha_a, \alpha_v, T) = \frac{1}{T}\left|\int_0^T \exp\left[\frac{im\omega_p}{c}\left(r_l - r_{l0} - \alpha_a t^2 - \alpha_v t\right)\right] dt\right| \tag{18}$$

and

$$\gamma_{3m}(\alpha_j, \alpha_a, \alpha_v, T) = \frac{1}{T}\left|\int_0^T \exp\left[\frac{im\omega_p}{c}\left(r_l - r_{l0} - \alpha_j t^3 - \alpha_a t^2 - \alpha_v t\right)\right] dt\right|. \tag{19}$$

For the general case of an orbit of eccentricity e, we have

$$r = a_p^{'}\left(1 - e^2\right)\left(1 + e\cos f\right)^{-1} \tag{20}$$

so that

$$r_0 = a_p^{'}\left(1 - e^2\right)\left(1 + e\cos f_0\right)^{-1}. \tag{21}$$

With this definition, Equations (13) and (14) become

$$r_l = a_p^{'}\left(1 - e^2\right)\left(1 + e\cos f\right)^{-1}\sin(f + \varpi), \tag{22}$$

and

$$r_{l0} = a_p^{'}\left(1 - e^2\right)\left(1 + e\cos f_0\right)^{-1}\sin(f_0 + \varpi). \tag{23}$$

Now, differentiating Equation (13) and using Equation (20) we get the expression for the velocity along the line of sight as

$$v_l = \dot{r_l} = \frac{2\pi}{P_o}\frac{a_p^{'}}{\sqrt{1 - e^2}}\left[\cos(f + \varpi) + e\cos(\varpi)\right], \tag{24}$$

where P_o is the orbital period of the pulsar and the orbital angular frequency is $\omega_o = 2\pi/P_o$. The quantities $a_p^{'}$ and P_o are related by Kepler's third law as

$$a_p^{'} = a_p \sin i = a_R \frac{M_c}{M_p + M_c}\sin i = \left[\left(\frac{P_o}{2\pi}\right)^2 G\left(M_p + M_c\right)\right]^{1/3}\frac{M_c}{M_p + M_c}\sin i, \tag{25}$$

where M_p is the mass of the pulsar and M_c is the mass of the companion and G is Newton's gravitational constant.

Differentiating Equation (24), we get the expression for the line-of-sight acceleration

$$a_l = \dot{v_l} = -\left(\frac{2\pi}{P_o}\right)^2 \frac{a_p^{'}}{\left(1 - e^2\right)^2}\sin(f + \varpi)\left(1 + e\cos f\right)^2. \tag{26}$$

Similarly, differentiating Equation (26), we get the expression for the line-of-sight jerk

$$j_l = -\left(\frac{2\pi}{P_o}\right)^3 \frac{a_p^{'}}{\left(1 - e^2\right)^{7/2}}\left(1 + e\cos f\right)^3\left[\cos(f + \varpi) + e\cos(\varpi) - 3e\sin(f + \varpi)\sin(f)\right]. \tag{27}$$

In principle, one can continue differentiating to get higher order derivatives (e.g. the "jounce" is the time derivative of the jerk). The expressions for v_l and a_l were previously derived by Freire, Kramer, & Lyne (2001, 2009). Assigning $f = f_0$ in Equations (24), (26) and (27) we get the values of v_{l0}, a_{l0} and j_{l0} respectively.

To compute Equations (17), (18) and (19) numerically, we need to solve Kepler's equations given below

$$M = \omega_o(t - T_p) \tag{28a}$$

$$E - e\sin E = M \tag{28b}$$

$$f = 2\tan^{-1}\left[\sqrt{\frac{1 + e}{1 - e}}\tan\frac{E}{2}\right], \tag{28c}$$

where M is the mean anomaly, E is the eccentric anomaly and T_p is the epoch of the periastron passage. $M_0 = -\omega_o T_p$, M_0

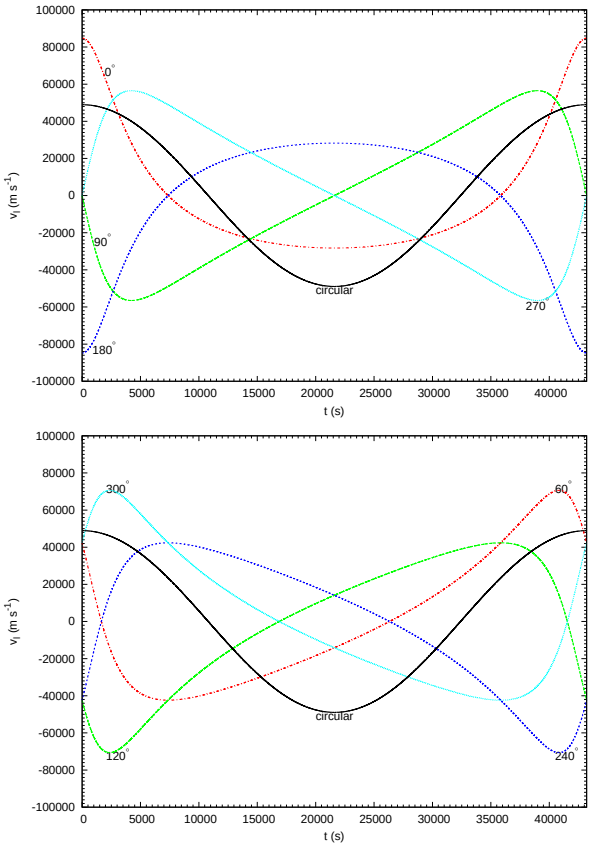

Figure 2. Variation of the line-of-sight velocity with time over a complete orbit for a binary pulsar with $M_p = 1.4\ M_\odot$, $M_c = 0.3\ M_\odot$, $P_o = 0.5$ day, $i = 60°$, $T_p = 0$, $e = 0.5$ for different ϖ, and the line-of-sight velocity for the same binary having zero eccentricity.

being the mean anomaly at $t = 0$. For a circular otbit, $e = 0$, $\varpi = 0$, $f = E = M$, giving $f = \omega_o t + f_0$, $f_0 = M_0 = -\omega_o T_p$ and we can get the expressions given by JK91 by substituting $A = a_p^{'}\omega_o$ and $\phi = f_0 + \pi/2$ (or if $\varpi = 270°$, $\phi = f_0$).

In Fig. 2, we plot the line-of-sight velocity with respect to time over a complete orbit for a binary pulsar with $M_p = 1.4\ M_\odot$, $M_c = 0.3\ M_\odot$, $P_o = 0.5$ day, $i = 60°$, $T_p = 0$, $e = 0.5$ for different ϖ between $0° - 360°$ and compare with the line-of-sight velocity plot in case of zero eccentricity. Like the circular case, line-of-sight velocity curve for the eccentric orbit is also symmetric over the half orbital period when ϖ is either $0°$, $90°$, $180°$ or $270°$ (upper panel), but not for any other values of ϖ (lower panel). In the lower panel of Fig. 2, ϖ is chosen to be $60°$, $120°$, $240°$ and $300°$, each in a different quadrant, but have the same average line-of-sight velocity over the entire orbit. The same can be found for other values of ϖ. That is why, in the next section, when we perform our analysis for different ϖ, we choose values only in the ranges of $0° - 90°$. The high value of eccentricity chosen here is justifiable as binary pulsars with eccentricity 0.5 or even higher exist in globular clusters, mainly as a result of stellar encounters (for a review, see Camilo & Rasio 2004).

For relativistic binaries, P_o, e, and ϖ change with time, and the rates of change of these parameters are classified as Post-Keplarian parameters. These changes need to be considered while performing pulsar timing analysis which involves pulse arrival times over a long span of time (days or even years); but, for the present study, we are concerned about the observability of pulsars, and these changes are negligible over the duration of any particular observation.

3 ANALYSIS

To demonstrate the impact of orbital motion on detectability, we will use the above framework to determine the maximum value of γ_{1m}, γ_{2m} and γ_{3m}. As different stellar and orbital parameters like P_p, P_o, M_c, M_p, $\sin i$, ϖ come into the equations given in Section 2, we perform our analysis for different values of these parameters. For a particular binary, the above parameters are fixed as the change in these parameters can be neglected over the duration of the observation. The orbital phase, i.e. the true anomaly f, is, however, not known a priori, and changes during the observation.

We divide the full-orbit (because of the asymmetry of an eccentric orbit which we have mentioned earlier) in equal steps of $10°$, having $f_{0,q}$s as $0°, 10°, 20° \ldots$ 350 (q going from 0 to 36), where $f_{0,q}$s are the values of the true anomaly at the start of the observation. For each $f_{0,q}$, we calculate $E_{0,q}$, $M_{0,q}$ and $T_{p,q}$ using Kepler's equations (28a, 28b, 28c). We use these $T_{p,q}$s

Table 1. Values of γ_{m1i} for different values of f_0 (true anomaly at the begining of the observation) and corresponding values of w for a binary with $M_p = 1.4\ M_\odot$, $M_c = 0.3\ M_\odot$, $i = 60°$, $\varpi = 0°$, $e = 0.5$, $P_p = 0.01$ s, $m = 4$, $T = 500$ s.

f_0	γ_{1m}	w
0°	0.28	0.111
10°	0.23	0.112
40°	0.19	0.131
50°	0.19	0.143
60°	0.21	0.160
70°	0.22	0.182
170°	0.98	0.970
180°	0.99	1.000
190°	0.86	0.970
350°	0.38	0.112

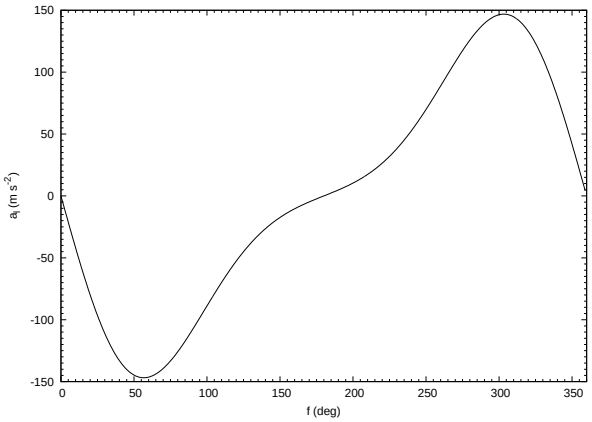

Figure 3. Variation of the line-of-sight acceleration with true anomaly over a complete orbit for a binary pulsar with $M_p = 1.4\ M_\odot$, $M_c = 0.3\ M_\odot$, $i = 60°$, $\varpi = 0°$, $e = 0.5$, $P_o = 0.1$ day.

to calculate M, E and f at any time t (between 0 and T) again solving equations (28a, 28b, 28c). This takes care of the change in orbital phase during the observation. Then we use Equations (24), (26) and (27) to get $\alpha_v = v_l(t)$, $\alpha_a = a_l(t)/2!$ and $\alpha_j = j_l(t)/3!$ for different choices of t between 0 and T and, for each set of α_v, α_a and α_j, we perform the integrations given in Equations (17), (18) and (19) numerically. The maximum values of of these integrations are the desired values γ_{m1q}, γ_{m2q} and γ_{m3q} respectively[1]. After this stage, we perform the weighted average of these efficiency factors over different $f_{0,q}$.

To perform this weighted average, we need to calculate the probability of each $f_{0,q}$ using the fact that the probability of a pulsar to be at a particular position in the orbit is directly proportional to the time it spends at that position. As the areal velocity is constant (Kepler's second law), the ratio of the time spent at true anomalies f_1 and f_2 can be expressed as $(1 + e\cos f_1)^{-2} : (1 + e\cos f_2)^{-2}$. So the weight factor w_q for each $f_{0,q}$ is given by $w_q = (1 + e\cos f_{0,q})^{-2}/(1 + e\cos f_{0,19})^{-2}$. $f_{0,19} = 180°$ corresponds to the apastron, where the pulsar spends most of its time. Using the values of γ_{m1q}s, γ_{m2q}s and γ_{m3q}s for each $f_{0,q}$, weighted averages can be estimated as:

$$\gamma_{m1,avg} = \frac{\sum_q w_q\,\gamma_{m1q}}{\sum_q w_q}, \qquad \gamma_{m2,avg} = \frac{\sum_q w_q\,\gamma_{m2q}}{\sum_q w_q}, \qquad \gamma_{m3,avg} = \frac{\sum_q w_q\,\gamma_{m3q}}{\sum_q w_q}, \qquad q = 1, 2 \ldots 36. \tag{29}$$

In this paper, we always report these average efficiency factors unless otherwise stated. We will henceforth skip the subscript avg, in section 4 and subsequent sections.

In Table 1, we show the values of γ_{m1q} for different values of f_0 and corresponding values of w for a binary with $M_p = 1.4\ M_\odot$, $M_c = 0.3\ M_\odot$, $i = 60°$, $\varpi = 0°$, $e = 0.5$, $P_o = 0.1$ day, $P_p = 0.01$ s, $m = 4$, $T = 500$ s. From Fig. 3, we see that a_l has the largest magnitude at $f = 57°$. Both $f_0 = 40°$ and $f_0 = 50°$ contains this value of f during the observation (the pulsar moves 20.83° during a 500 s long observation), so we get the smallest value of γ_{m1i} here. Note that although $f_0 = 170°$ and $f_0 = 190°$ are equally likely (same value of w) and correspond to the same value of a_l, but as the values of a_l during next 500 s are different, they give different values for γ_{1m}. Similarly, both $f = 0°$ and $f = 180°$ correspond to $a_l = 0$, but the values of a_l during next 500 sec after $f_0 = 0°$ and $f_0 = 180°$ are different, so they result different values of γ_{1m}.

[1] Remember that only α_v comes in the expression for γ_{m1q}, and only α_a and α_v come in the expression of γ_{m2q}.

4 RESULTS

4.1 Neutron Star - White Dwarf (NS-WD) Binaries

If the neutron star is a recycled millisecond pulsar, then the orbit is expected to be circular because of the strong tidal phase in the past when the neutron star accreted matter from the companion (Alpar *et al.* 1982; Radhakrishnan & Srinivasan 1982). However, in dense stellar environments like globular clusters or nuclear star clusters near the Galactic center, stellar interactions lead to eccentric orbits for recycled pulsar binaries. Many such systems in globular clusters are known at present[2]. Moreover, three body interactions can also produce millisecond pulsars in eccentric orbit. One such system is PSR J1903+0327, which was a member of a triple system in the past, but has become a binary by ejecting one member of the system (Champion *et al.* 2008; Portegies Zwart *et al.* 2011). Fig. 2 shows the line-of-sight velocity plots for a canonical example of this category.

It is clear from Equation (9), that the spread of the power among adjacent Fourier bins is larger for higher values of m or larger values of ω_p, thus the values of the efficiency factors decrease for higher m or smaller P_p. Similarly, a smaller value of P_o gives higher values of v_l, a_l and j_l and so on (all other parameters being fixed) resulting in a larger spread of the power among adjacent Fourier bins, *i.e.*, reduction of the efficiency factors. It is evident from Eqn. (25) that higher value of $\sin i$ will increase the values of v_l, a_l, j_l and so on, leading to a decrease in the efficiency factors. To demonstrate these facts graphically, we show variations of γ_{1m} with with P_o and P_s for different parameters. In all the subsequent plots, the X-axis shows the values of P_p, the Y-axis shows the values of P_o and the color code represents the values of γ_{1m}. The contour for $\gamma_{1m} = 0.5$ is also shown in each plot. We can say that the pulsars having $\gamma_{1m} < 0.5$ (lying on the bottom-left side of the $\gamma_{1m} = 0.5$ contour) are difficult to detect. Fig. 4 shows the variation for different values of ϖ. We see that the $\gamma_{1m} = 0.5$ contour shifts rightward with the increase of ϖ, making a larger portion of the phase-space difficult to detect. Fig. 5 shows the variation for different values of i, and as expected, the increase of i makes a larger portion of the phase-space difficult to detect. In Fig. 6, we show variations of γ_{1m} with with P_o and P_s for different M_c keeping all other parameters fixed, and we see that the values of γ_{1m} are lower for higher values of M_c when all other parameters are the same. This happens because a_p increases with the increase of M_c (if P_o remains the same) giving higher values of v_l, a_l and j_l etc. resulting in a larger spread of the power among adjacent Fourier bins, *i.e.*, reduction of the efficiency factors. As an example, if M_c increases from 0.1 $M_\odot$ to 0.8 $M_\odot$, the fractional increase in a_p is 5.2. On the other hand, from Fig 7, we have not seen any significant effect of the variation of M_p in the realistic range of $1 - 2$ $M_\odot$, because the fractional increase of a_p is only 0.32 when M_p increases from 1 $M_\odot$ to 2 $M_\odot$. In Fig. 8, we show variations of γ_{1m} with with P_o and P_s for different values of e and find that it does not play any significant role unless very high when γ_{1m} increases with the increase of e. In Fig. 9, we show the variations of γ_{1m} with with P_o and P_s for $m = 1$ and $m = 7$ keeping all the other parameters fixed and, as expected, γ_{1m} decreases for higher values of m. In Fig. 10, we show variations of γ_{1m} with with P_o and P_s for different values of T and find that a smaller value of T makes a larger portion of the phase space easy to detect. This fact was also noticed by Ramachandran & Portegies Zwart (1998). On the other hand, smaller T reduces the value of minimum detectable flux density for a pulsar, independent of its orbital parameters (Lorimer & Kramer 2005). Hence an optimal strategy is needed to choose a value of T depending upon the motivation of the survey and efficiency of the telescope.

In Fig. 11, we show variation of γ_{2m} and γ_{3m} with P_o and P_s keeping $\varpi = 30^\circ$, $i = 60^\circ$ $M_p = 1.4$ $M_\odot$, $M_c = 0.3$ $M_\odot$, $m = 4$ and $T = 1000$ s. These can be compared to Fig. 4(b) which shows the variation of γ_{1m} for the same set of parameters. The increases in efficiency factors by using acceleration or acceleration-jerk searches are significant. We notice that the slope of the contour is different and the use of acceleration or acceleration-jerk searches are more effective for short orbital periods. This result agrees with that obtained by JK91.

In Table 3, we present the efficiency factors for $T = 1000$ s and $m = 4$, averaged over different f_0s as described earlier for the NS-WD binaries for which all the required parameters, e.g., P_p, e, P_o, $\sin i$, ϖ, M_c and M_p are known, for few cases, the values of M_p are not known, so assumed to be 1.4 $M_\odot$. Table 2 shows the parameters for these binaries and corresponding references.

For the sake of simplicity, in most cases, we compute the efficiency factors for the $m = 4$ harmonic, but the procedure will be the same for any other harmonic. The value of the efficiency factor at any harmonic m_2 for spin period P_{p_2} would be the same as that at the harmonic m_1 and spin period P_{p_1} if $P_{p_2} = \frac{m_2}{m_1} P_{p_1}$ if we keep all other parameters unchanged. This fact can be used to read the efficiency factors for any other harmonic from the plots.

In the case of a real pulsar, the number of harmonics present in the Fourier spectrum of a pulse is roughly reciprocal of the pulse duty cycle (Lorimer & Kramer 2005). Harmonic summing is used to get the power from each of these harmonics. The power of lower harmonics are higher as well as the efficiency factors. As a combined effect, the contributions from higher harmonics become more significant for a binary pulsar. An an example, we fit the pulse profile of PSR J1802−2124 (Faulkner *et al.* 2004) with a Gaussian, and compute the Fourier spectrum. Table 4 shows the values of γ_{1m} for first 10 harmonics, power (D_m) of each harmonic (in arbitrary unit) and degraded power ($\gamma_{1m}^2 D_m$) of each harmonic for different

[2] http://www.naic.edu/∼pfreire/GCpsr.html

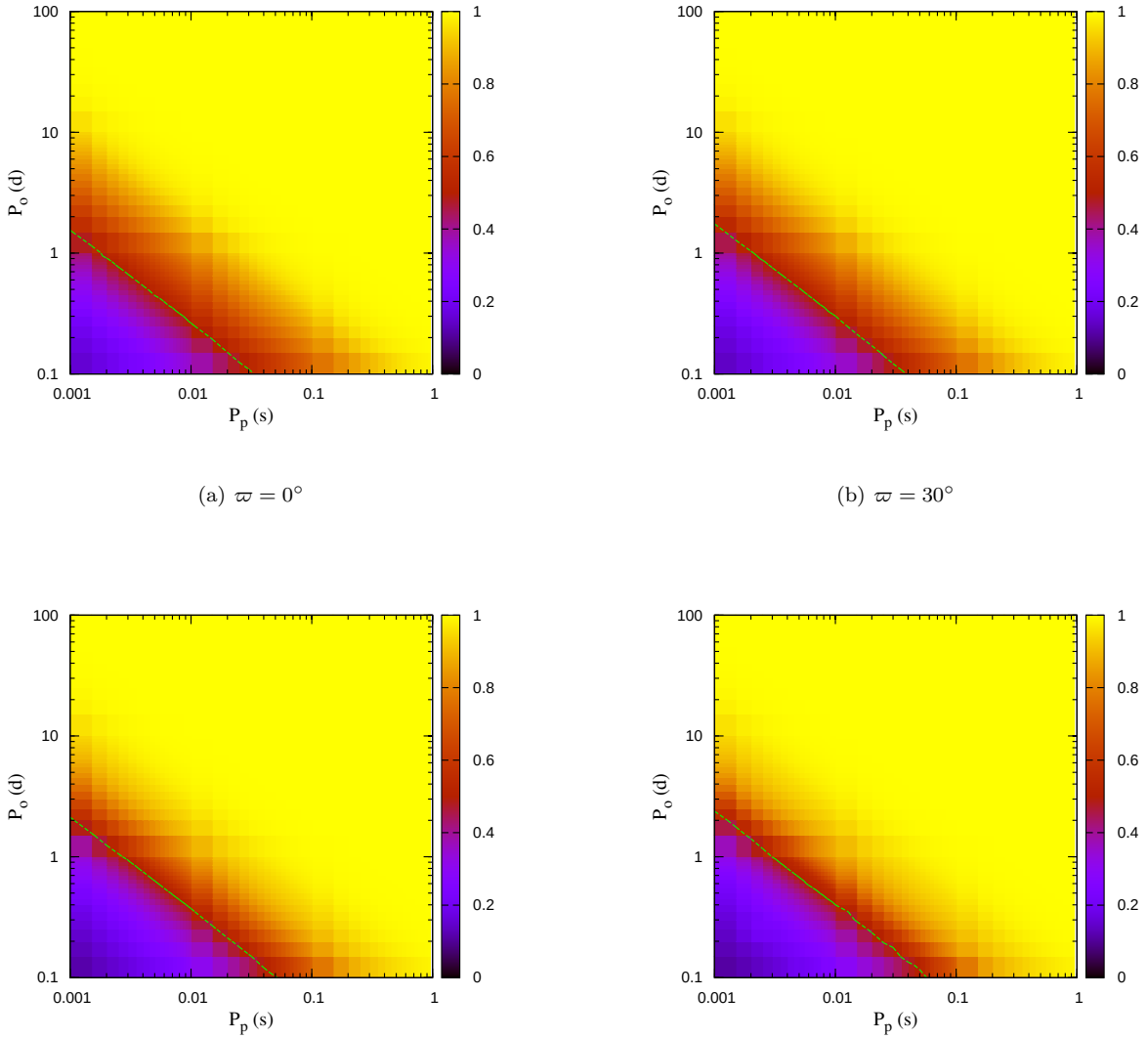

(a) $\varpi = 0°$ (b) $\varpi = 30°$

(c) $\varpi = 60°$ (d) $\varpi = 90°$

Figure 4. Variation of γ_{1m} with P_o and P_s for different ϖ. For each case, $i = 60°$, $M_p = 1.4\ M_\odot$, $M_c = 0.3\ M_\odot$, $e = 0.5$, $m = 4$, $T = 1000$ s.

observation duration, e.g. T =500, 100, 1500 and 2000 s. As expected, for any fixed value of T, γ_{1m} decreases with increasing value of m, and for any fixed value of m, γ_{1m} decreases with the increase of T. Note that, for any fixed value of T, the decrease in the value of $\gamma_{1m}^2\, D_m$ from $m = 1$ to $m = 10$ is slower than that of D_m.

4.2 Double Neutron Star (DNS) Binaries

Presently there are eight confirmed double neutron star (DNS) binaries and four more candidate DNSs. Among these twelve, all required parameters to calculate efficiency factors are known only for four. We present the efficiency factors for these DNSs in Table 6, for $T = 1000$ s, $m = 4$. The parameters for these DNSs with corresponding references are given in Table 5.

In Fig. 12 we show the line-of-sight velocity curves for a hypothetical DNS having $M_p = 1.35\ M_\odot$, $M_c = 1.25\ M_\odot$, $P_o = 0.5$ day, $i = 60°$, $T_p = 0$, $e = 0.5$ for different ϖ. DNS systems can have such high eccentricity and short orbital period. One example is the Hulse-Taylor binary PSR B1913+16, which has $e = 0.617$ and $P_o = 0.323$ day. Comparing Fig. 12 with Fig. 2, we see that the amplitudes of radial velocity curves are ~ 3 times larger for a DNS in comparison with a NS-WD binary

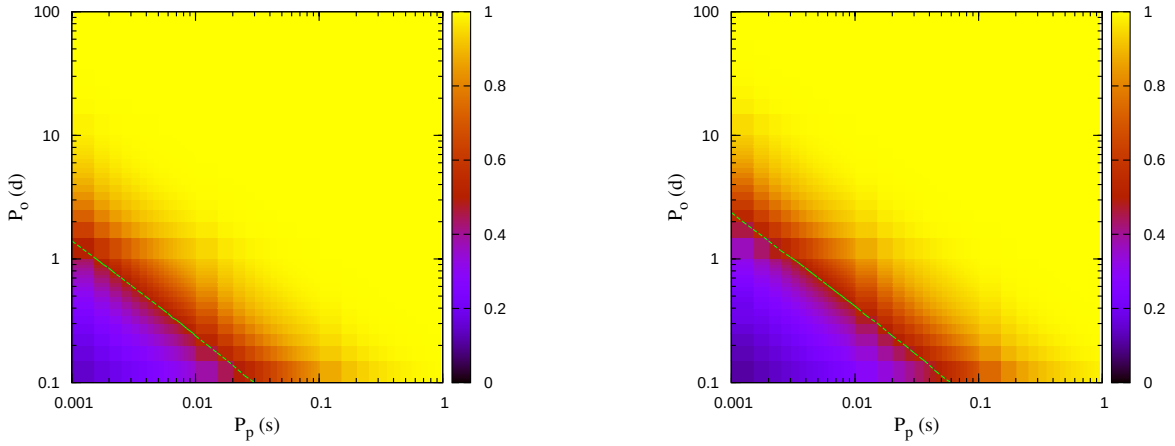

(a) $i = 30°$ (b) $i = 90°$

Figure 5. Variation of γ_{1m} with P_o and P_s for different i. For each case, $\varpi = 60°$, $M_p = 1.4\ M_\odot$, $M_c = 0.3\ M_\odot$, $e = 0.5$, $m = 4$, $T = 1000$ s.

Table 2. Parameters for NS-WD binaries for which we can calculate efficiency factors. The columns from left to right show the name of the pulsar, spin period, orbital period, orbital eccentricity, sine of the inclination angle, longitude of periastron, companion mass, pulsar mass and corresponding references.

Pulsar	P_p (sec)	P_o (day)	e	$\sin i$	ϖ (deg)	M_c ($M_\odot$)	M_p ($M_\odot$)	Refs.
J0437−4715	0.005757	5.74105	1.918×10^{-5}	0.674	1.222	0.254	1.76	Verbiest *et al.* (2008)
J0751+1807	0.003479	0.26314	5.0×10^{-7}	0.9121	45.0	0.191	1.26	Nice *et al.* (2005); ATNF catlogue‡ for ϖ Nice, Stairs, & Kasian (2007, for M_p)
J1600−3053	0.003598	14.34846	17.369×10^{-5}	0.8	181.85	0.6	1.4*	Verbiest *et al.* (2009)
J1603−7202	0.014842	6.30863	9.3×10^{-6}	0.89	169	0.14	1.4*	Hotan, Bailes, & Ord (2006)
J1614−2230	0.003151	8.68662	1.30×10^{-6}	0.9999	175.1	0.500	1.97	Demorest *et al.* (2010)
J1640+2224	0.003163	175.46066	7.973×10^{-4}	0.99	50.731	0.15	1.4*	Löhmer *et al.* (2005)
J1713+0747	0.00457	67.82513	7.494×10^{-5}	0.95	176.191	0.28	1.3	Splaver *et al.* (2005)
J1738+0333	0.00585	0.35479	3.4×10^{-7}	0.5388	155.695	0.19	1.46	Freire *et al.* (2012)
J1802−2124	0.012648	0.69889	2.48×10^{-6}	0.9845	20.0	0.78	1.24	Ferdman *et al.* (2010)
J1903+0327	0.00215	95.17412	0.4367	0.976	141.652	1.03	1.67	Freire *et al.* (2011)

‡ : http://www.atnf.csiro.au/research/pulsar/psrcat/expert.html
* : M_p not measured, taken as 1.4 $M_\odot$

Table 3. Efficiency factors and corresponding parameters for NS-WD binaries (for which all required parameters are known) for $T = 1000$ s, $m = 4$ (averaged over different T_ps as described in the text).

pulsar	γ_{1m}	γ_{2m}	γ_{3m}
J0437−4715	1.00	1.00	1.00
J0751+1807	0.29	0.64	0.98
J1600−3053	1.00	1.00	1.00
J1603−7202	1.00	1.00	1.00
J1614−2230	0.99	1.00	1.00
J1640+2224	1.00	1.00	1.00
J1713+0747	1.00	1.00	1.00
J1738+0333	0.56	0.95	1.00
J1802−2124	0.50	0.98	1.00
J1903+0327	1.00	1.00	1.00

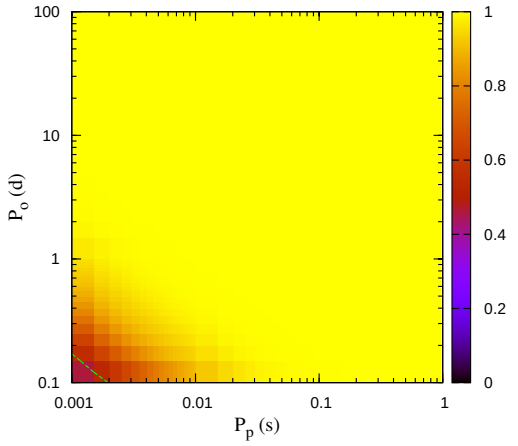

(a) $M_c = 0.01\ M_\odot$

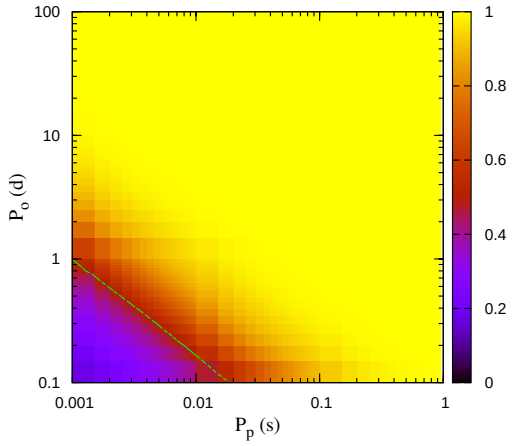

(b) $M_c = 0.1\ M_\odot$

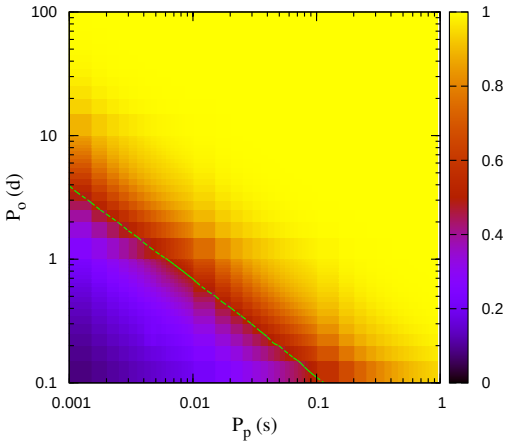

(c) $M_c = 0.8\ M_\odot$

Figure 6. Variation of γ_{1m} with P_o and P_s for different M_c. For each case, $i = 60°$, $\varpi = 60°$, $M_p = 1.4\ M_\odot$, $e = 0.5$, $m = 4$, $T = 1000$ s.

Table 4. Values of γ_{1m} for first 10 harmonics of PSR J1802−2124, power (D_m) of each harmonic (in arbitrary unit) and degraded power ($\gamma_{1m}^2\ D_m$) of each harmonic for T =500, 100, 1500 and 2000 s. The pulse profile was fitted with a Gaussian.

		$T = 500$ s		$T = 1000$ s		$T = 1500$ s		$T = 2000$ s	
harmonic number (m)	power (D_m)	γ_{1m}	$\gamma_{1m}^2\ D_m$	γ_{1m}	$\gamma_{1m}^2\ D_m$	γ_{1m}	$\gamma_{1m}^2\ D_m$	γ_{1m}	$\gamma_{1m}^2\ D_m$
1	1.00000	0.99	0.982998	0.87	0.761651	0.64	0.412938	0.51	0.257970
2	0.88965	0.97	0.830733	0.67	0.400844	0.48	0.206042	0.38	0.128296
3	0.62585	0.93	0.536621	0.57	0.203214	0.41	0.103509	0.31	0.060903
4	0.34728	0.87	0.264492	0.50	0.088176	0.36	0.043970	0.27	0.025762
5	0.15156	0.81	0.099354	0.46	0.031453	0.32	0.015686	0.25	0.009186
6	0.05199	0.74	0.028554	0.42	0.009198	0.30	0.004363	0.23	0.002693
7	0.01412	0.70	0.006924	0.39	0.002202	0.27	0.001009	0.22	0.000674
8	0.00310	0.67	0.001394	0.38	0.000441	0.25	0.000196	0.20	0.000125
9	0.00056	0.64	0.000230	0.35	0.000070	0.24	0.000032	0.19	0.000020
10	0.00008	0.61	0.000029	0.34	0.000009	0.23	0.000004	0.18	0.000003

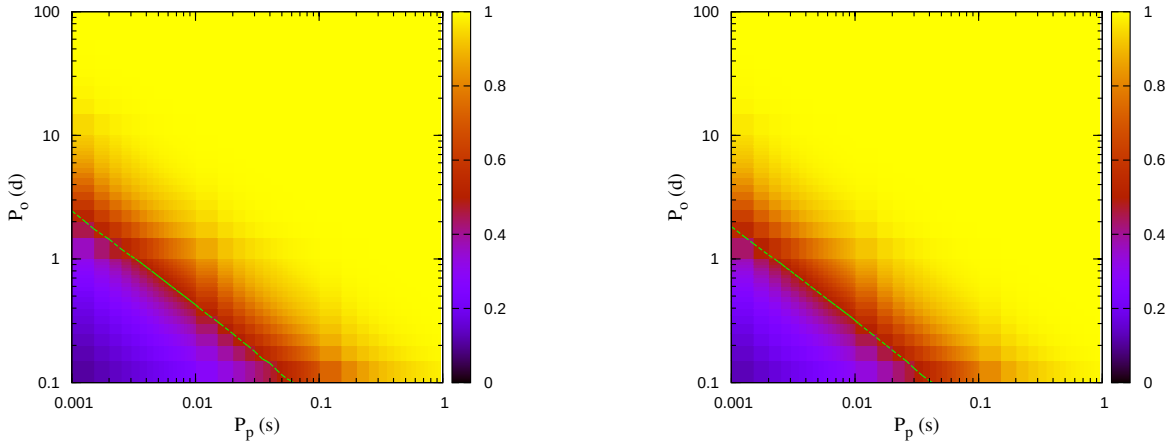

(a) $M_p = 1.0 M_\odot$ (b) $M_p = 2.0\ M_\odot$

Figure 7. Variation of γ_{1m} with P_o and P_s for different M_p. For each case, $i = 60°$, $\varpi = 60°$, $M_c = 0.3\ M_\odot$, $e = 0.5$, $m = 4$, $T = 1000$ s.

Table 5. Parameters for the DNSs for which we can calculate efficiency factors. The columns from left to right show the name of the pulsar, spin period, orbital period, orbital eccentricity, sine of the inclination angle, longitude of periastron, companion mass, pulsar mass and corresponding references.

DNS	P_p (sec)	P_o (day)	e	$\sin i$	ϖ (deg)	M_c ($M_\odot$)	M_p ($M_\odot$)	Refs.
J0737−3039A	0.022699	0.10225	0.08778	0.9997	87.033	1.249(B)	1.338(A)	Kramer *et al.* (2006)
J0737−3039B	2.773461	0.10225	0.08778	0.9997	267.033	1.338(A)	1.249(B)	Kramer *et al.* (2006)
B1534+12	0.037904	0.42074	0.27368	0.975	274.769	1.35	1.328	Konacki *et al.* (2003); Stairs *et al.* (2002, for M_{tot})
J1756−2251	0.028461	0.31963	0.18057	0.95	327.825	1.312	1.258	Ferdman (2008)
J1807−2500B†	0.004186	9.95667	0.74703	0.996	11.335	1.206	1.365	Lynch *et al.* (2012)
B1913+16	0.059030	0.32300	0.61713	0.71	292.545	1.389	1.440	Weisberg, Nice, & Taylor (2010); Damour & Shäfer (1988, for $\sin i$)

† : candidate DNS.

having the same values of P_o, e, $\sin i$ and ϖ. This fact leads to a reduction in the efficiency factors for DNSs in comparison with NS-WD binaries.

In Fig 13, we show the variations of γ_{1m}, γ_{2m}, and γ_{3m} with P_o and P_s for $M_p = 1.35\ M_\odot$, $M_c = 1.25\ M_\odot$, $\varpi = 30°$, $i = 60°$, $e = 0.5$, $m = 4$, and $T = 1000$ s. The variations of γ_{1m} with P_o and P_s for $e = 0.1$ and $e = 0.8$ keeping all other parameters unchanged are shown in Fig 14. Again, it is clear that a higher value of eccentricity is favourable for detection, i.e. results a higher value of γ_{1m}. This fact was also observed by Ramachandran & Portegies Zwart (1998), who studied eccentric systems only for DNS binaries.

Table 6. Efficiency factors for DNSs (for which all required parameters are known) for $T = 1000$ s, $m = 4$.

DNS	γ_{1m}	γ_{2m}	γ_{3m}
J0737−3039A	0.21	0.41	0.56
J0737−3039B	0.98	1.00	1.00
B1534+12	0.52	0.92	1.00
J1756−2251	0.41	0.85	0.99
J1807−2500B	0.92	1.00	1.00
B1913+16	0.68	0.92	0.94

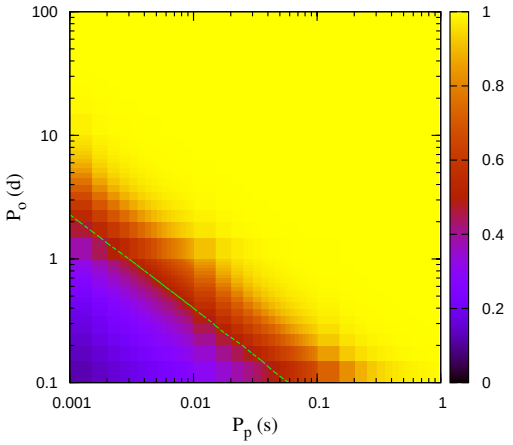

(a) $e = 0.001$

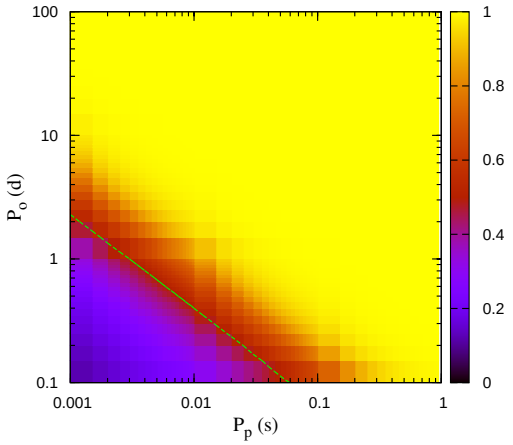

(b) $e = 0.01$

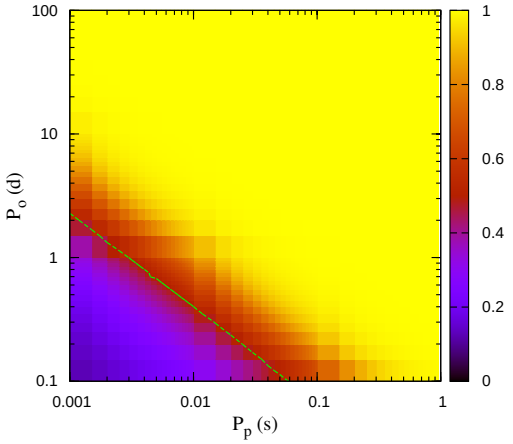

(c) $e = 0.1$

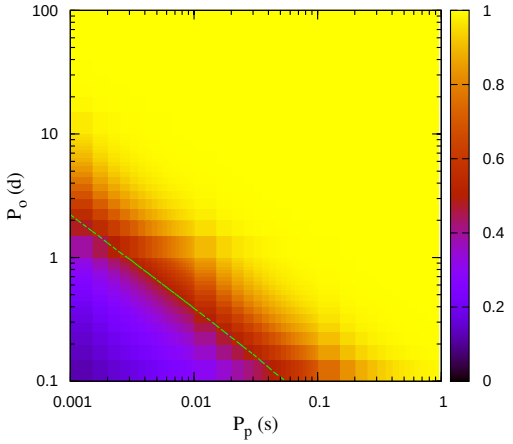

(d) $e = 0.3$

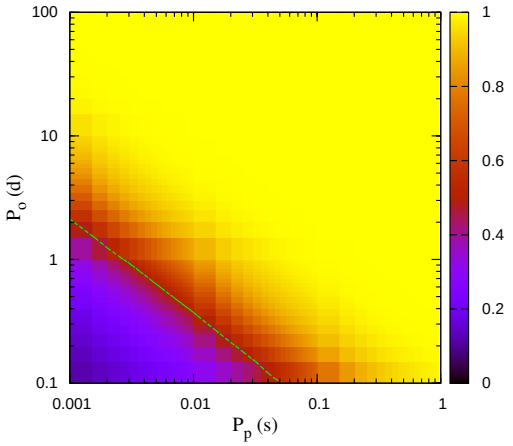

(e) $e = 0.5$

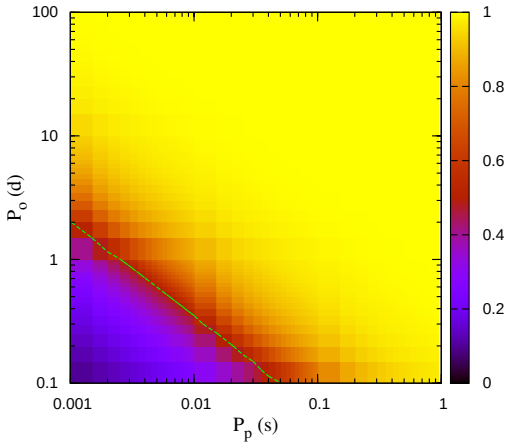

(f) $e = 0.8$

Figure 8. Variation of γ_{1m} with P_o and P_s for different e. For each case, $i = 60°$, $\varpi = 60°$, $M_p = 1.4\ M_\odot$, $M_c = 0.3\ M_\odot$, $m = 4$and $T = 1000$ s.

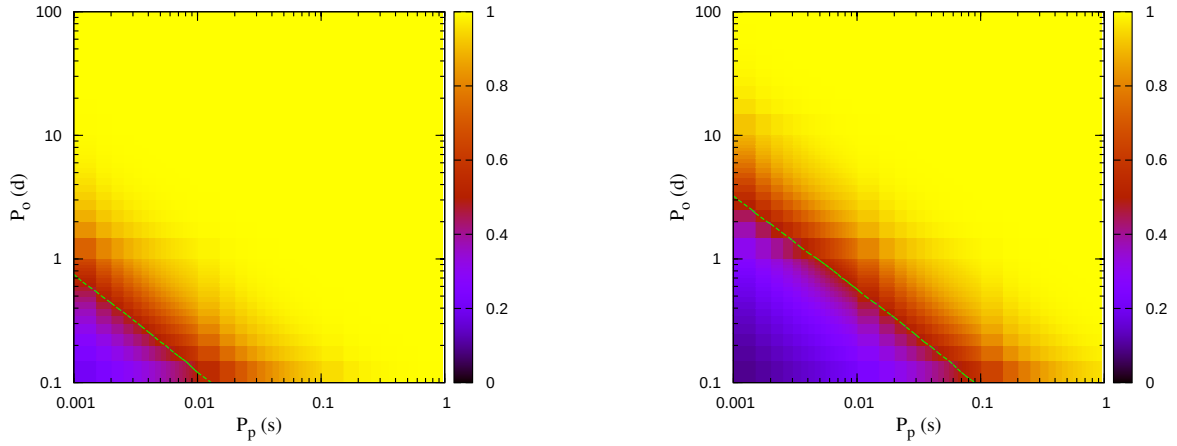

(a) $m = 1$ (b) $m = 7$

Figure 9. Variation of γ_{1m} with P_o and P_s for different m. For each case, $\varpi = 60°$, $i = 60°$, $M_p = 1.4\ M_\odot$, $M_c = 0.3\ M_\odot$, $e = 0.5$and $T = 1000$ s.

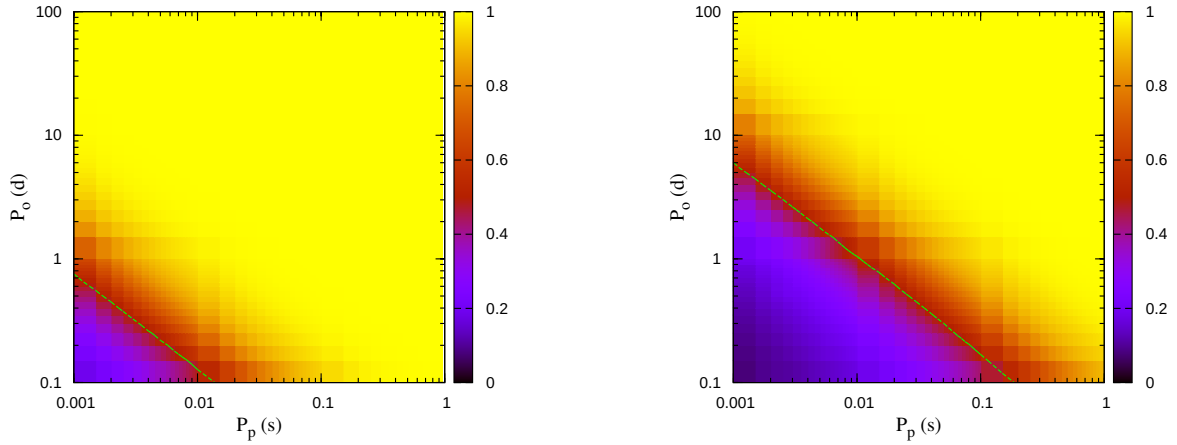

(a) $T = 500$ s (b) $T = 2000$ s

Figure 10. Variation of γ_{1m} with P_o and P_s for different T. For each case, $\varpi = 60°$, $i = 60°$, $M_p = 1.4\ M_\odot$, $M_c = 0.3\ M_\odot$, $e = 0.5$, $m = 4$.

4.3 Neutron Star - Black Hole (NS-BH) Binaries

Although no neutron star - (stellar mass) black hole (NS-BH) binary is known at present, there is high possibility of detecting such systems with forthcoming facilities like SKA (Smits *et al.* 2009).

A number of theoretical studies (Pfahl, Podsiadlowski, & Rappaport 2005; Kiel & Hurley 2009; Faucher-Giguére & Loeb 2011) exist which predict probable parameters for these systems. The population synthesis model of Pfahl, Podsiadlowski, & Rappaport (2005) predicts mildly recycled pulsars in short orbits (P_o in the range of $0.004 - 0.8$ days) with small eccentricities, while the study by Kiel & Hurley (2009) predicts recycled pulsars with orbital periods ranging from 0.1 days to 10^5 days. Faucher-Giguére & Loeb (2011) found that recycled pulsars with black hole companions in highly eccentric orbits with P_o between 0.003 and 0.6 days can form due to stellar encounters in dense stellar environments. In this work, we calculate the

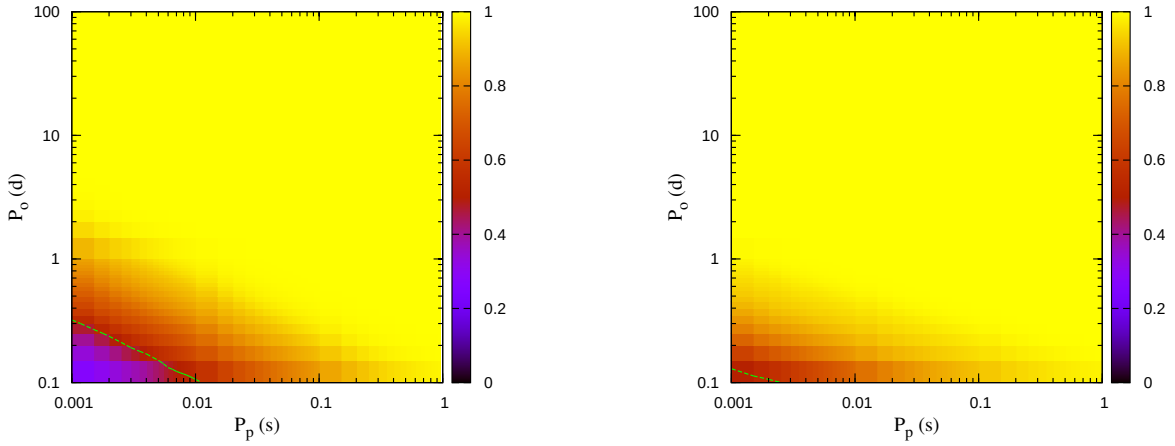

(a) γ_{2m} (b) γ_{3m}

Figure 11. Variations of γ_{2m} and γ_{3m} with P_o and P_s keeping $\varpi = 30°$, $i = 60°$ $M_p = 1.4\ M_\odot$, $M_c = 0.3\ M_\odot$, $m = 4$ and $T = 1000$ s.

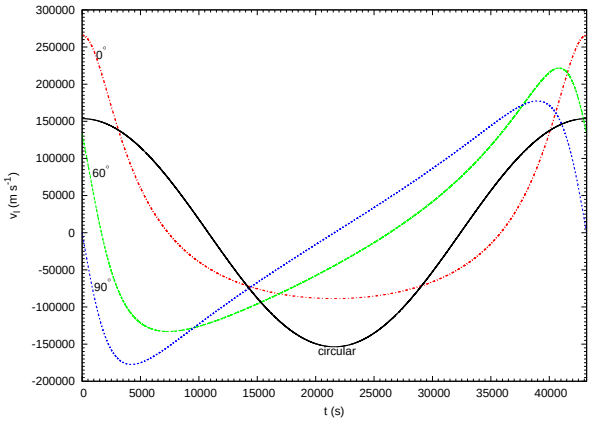

Figure 12. Variation of the line-of-sight velocity with time over a complete orbit for a DNS, having $M_p = 1.35\ M_\odot$, $M_c = 1.25\ M_\odot$, $P_o = 0.5$ day, $i = 60°$, $T_p = 0$, $e = 0.5$ for different ϖ, and the line-of-sight velocity for the same binary having zero eccentricity.

efficiency factors for $0.1 < P_o < 100$ days and $0.001 < P_p < 1$, as we chose for the cases of NS-WD and NS-NS binaries. We take the mass of the black hole as 10 $M_\odot$, which agrees with the observations (Farr *et al.* 2011).

In Fig. 15, we show the variation of the radial velocity with time for a NS-BH binary with $M_p = 1.4\ M_\odot$, $M_c = 10.0\ M_\odot$, $P_o = 0.5$ day, $i = 60°$, $T_p = 0$, $e = 0.5$ for different ϖ, as well as the circular case (keeping all other parameters fixed). We see that the amplitudes of the line-of-sight velocity curves are ~ 3 times larger for a NS-BH in comparison with a NS-NS binary having the same values of P_o, e, $\sin i$ and ϖ (or ~ 9 times larger for a NS-BH in comparison with a NS-WD binary). So it is clear that $T = 1000$ s is too high for this case and will lead to very small efficiency factors and we decided to use $T = 500$ s.

In Fig. 16, we show the variations of γ_{1m}, γ_{2m}, and γ_{3m} with P_o and P_s for $\varpi = 30°$, $i = 60°$, $e = 0.5$, $m = 4$, and $T = 1000$ s. The variations of γ_{1m} with P_o and P_s for $e = 0.1$ and $e = 0.8$ keeping all other parameters unchanged are shown in Fig 17. A higher value of eccentricity is favourable for detection, i.e. results a higher value of γ_{1m}.

5 CONCLUSIONS

We have generalized the earlier work of JK91 to calculate the signal-to-noise degradation of pulsars in binary orbits with arbitrary eccentricity. We have applied the framework to compute degradation factors for a variety of orbital configurations, and show that it can be quite substantial. We have also demonstrated how the degradation can be recovered by using acceleration search or acceleration-jerk search algorithms. The analysis should prove invaluable to a wide variety of popula-

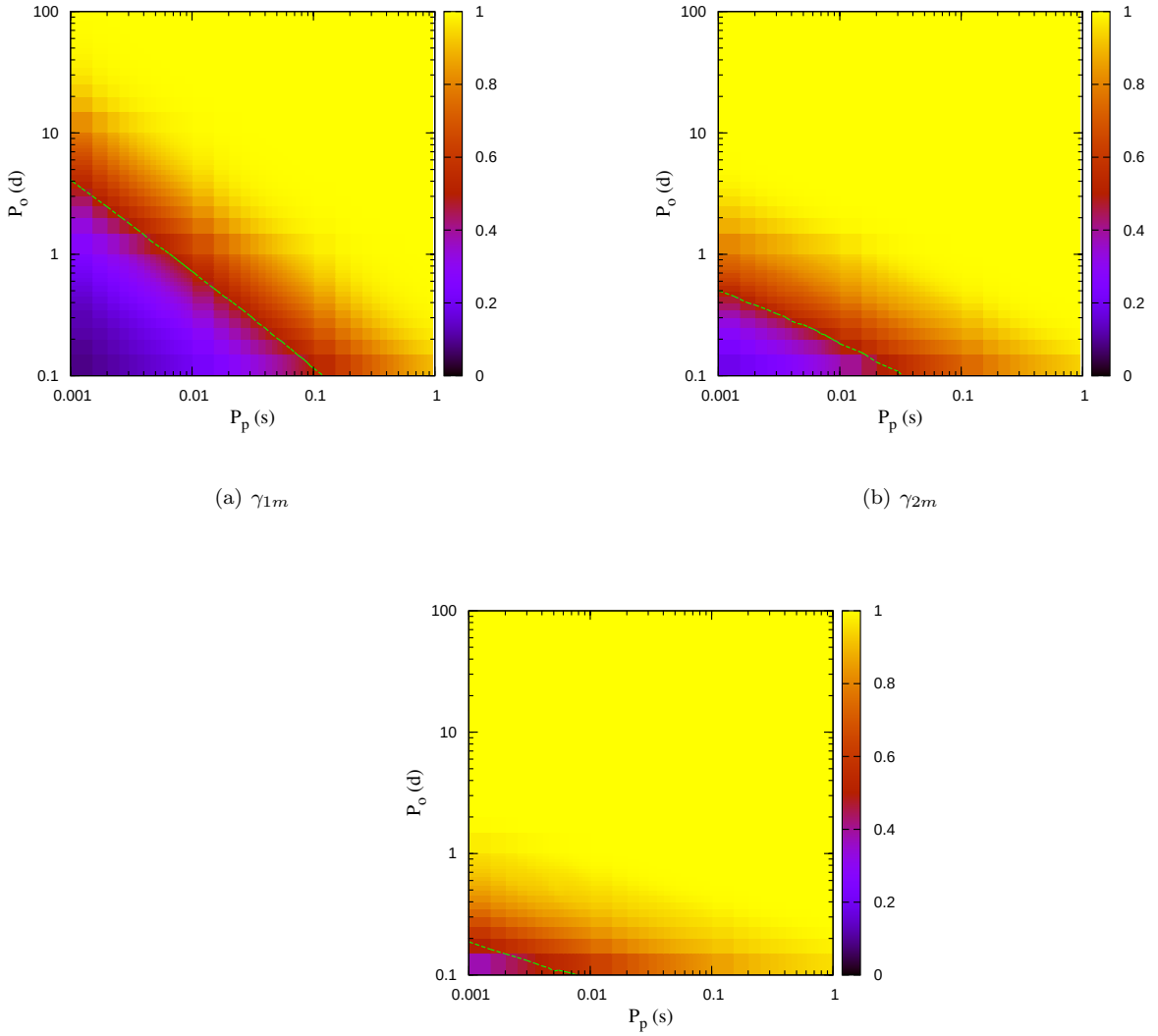

(a) γ_{1m}

(b) γ_{2m}

(c) γ_{3m}

Figure 13. Variation of γ_{1m}, γ_{2m}, and γ_{3m} with P_o and P_s for $M_p = 1.35\ M_\odot$,$M_c = 1.25\ M_\odot$, $\varpi = 30°$, $i = 60°$, $e = 0.5$, $m = 4$, and $T = 1000$ s.

tion studies since this work provides, for the first time, accurate accounting for this important effect. Software to calculate the degradation factors for arbitarary orbital parameters, harmonic summing and survey integrations is available online at http://psrpop.phys.wvu.edu/binary.

ACKNOWLEDGEMENTS

This work was supported by a Research Challenge Grant to the WVU Center for Astrophysics by the West Virginia EPSCoR foundation, and also from the Astronomy and Astrophysics Division of the National Science Foundation via a grant AST-0907967.

REFERENCES

Anderson, S. B., 1993, Ph. D Thesis, California Institute of Technology
Alpar, M. A., Cheng, A. F., Ruderman, M. A., Shaham, J., 1982, Nature, 300, 728

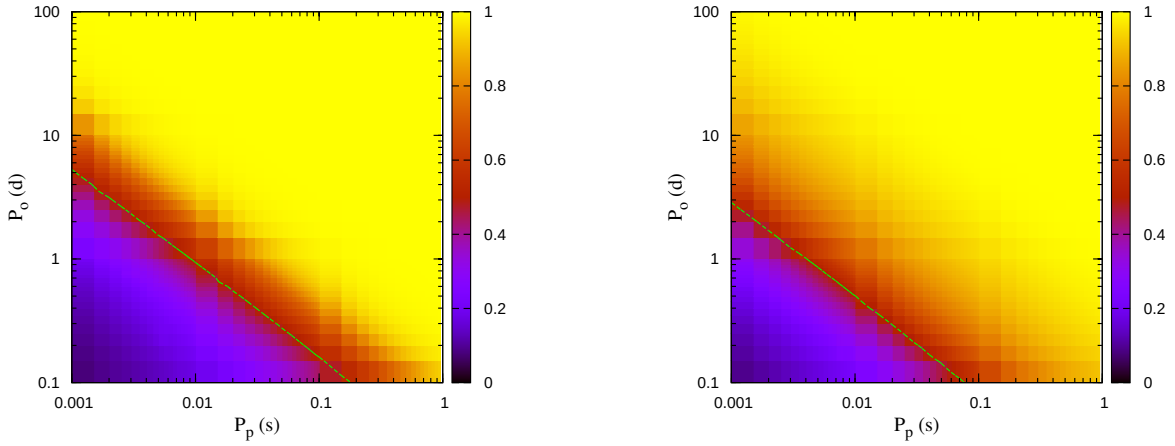

(a) $e = 0.1$ (b) $e = 0.8$

Figure 14. Variation of γ_{1m} with P_o and P_s for $M_p = 1.35\ M_\odot$, $M_c = 1.25\ M_\odot$, $\varpi = 30°$, $i = 60°$, $m = 4$, and $T = 1000$ s, for $e = 0.1$ and $e = 0.8$.

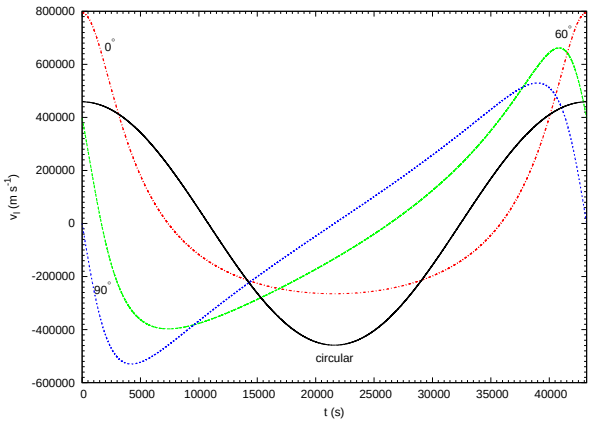

Figure 15. Variation of the line-of-sight velocity with time over a complete orbit for a binary pulsar with a black hole companion with $M_p = 1.4\ M_\odot$, $M_c = 10.0\ M_\odot$, $P_o = 0.5$ day, $i = 60°$, $T_p = 0$ and $e = 0.5$ for different ϖ, and the line-of-sight velocity for the same binary having zero eccentricity.

Champion, D. J., Ransom, S. M., Lazarus, P., *et al.*, 2008, Science, 320, 1309
Damour, T., & Shäfer, G., 1988, Nuovo Cimento B, 101, 127.
Demorest, P. B., Pennucci, T., Ransom, S. M., Roberts, M. S. E. & Hessels, J. W. T., 2010, Nature, 467, 1081
Farr, W. M., Sravan, N., Cantrell, A., Kreidberg, L., Bailyn, C. D., Mandel, I., Kalogera, V., 2011, ApJ, 741, 103
Faucher-Giguére, C.; Loeb, A., 2011, MNRAS, 415, 395
Faulkner, A. J., Stairs, I. H., Kramer, M., *et al.*, 2004, MNRAS, 355, 147
Ferdman, R. D., 2008, Ph. D. Thesis, University of British Columbia
Ferdman, R. D., Stairs, I. H., Kramer, M., 2010, ApJ, 711, 764
Freire, P. C. C., Bassa, C. G., Wex, N., *et al.*, 2011, MNRAS, 412, 2763
Freire, P. C., Kramer, M., Lyne, A. G., 2001, MNRAS, 322, 885
Freire, P. C., Kramer, M., Lyne, A. G., 2009, MNRAS, 395, 1775
Freire, P. C., Wex, N., Esposito-Farese, G., *et al.*, 2012, MNRAS, 423, 3328
Hotan, A. W., Bailes, M., & Ord, S. M., 2006, MNRAS, 369, 1502
Johnston, H. M., & Kulkarni, S. R., 1991, ApJ, 368, 504
Kiel, P. D., Hurley, J. R., 2009, MNRAS, 395, 2326
Konacki, M., Wolszczan, A., Stairs, I. H., 2003, ApJ, 589, 495

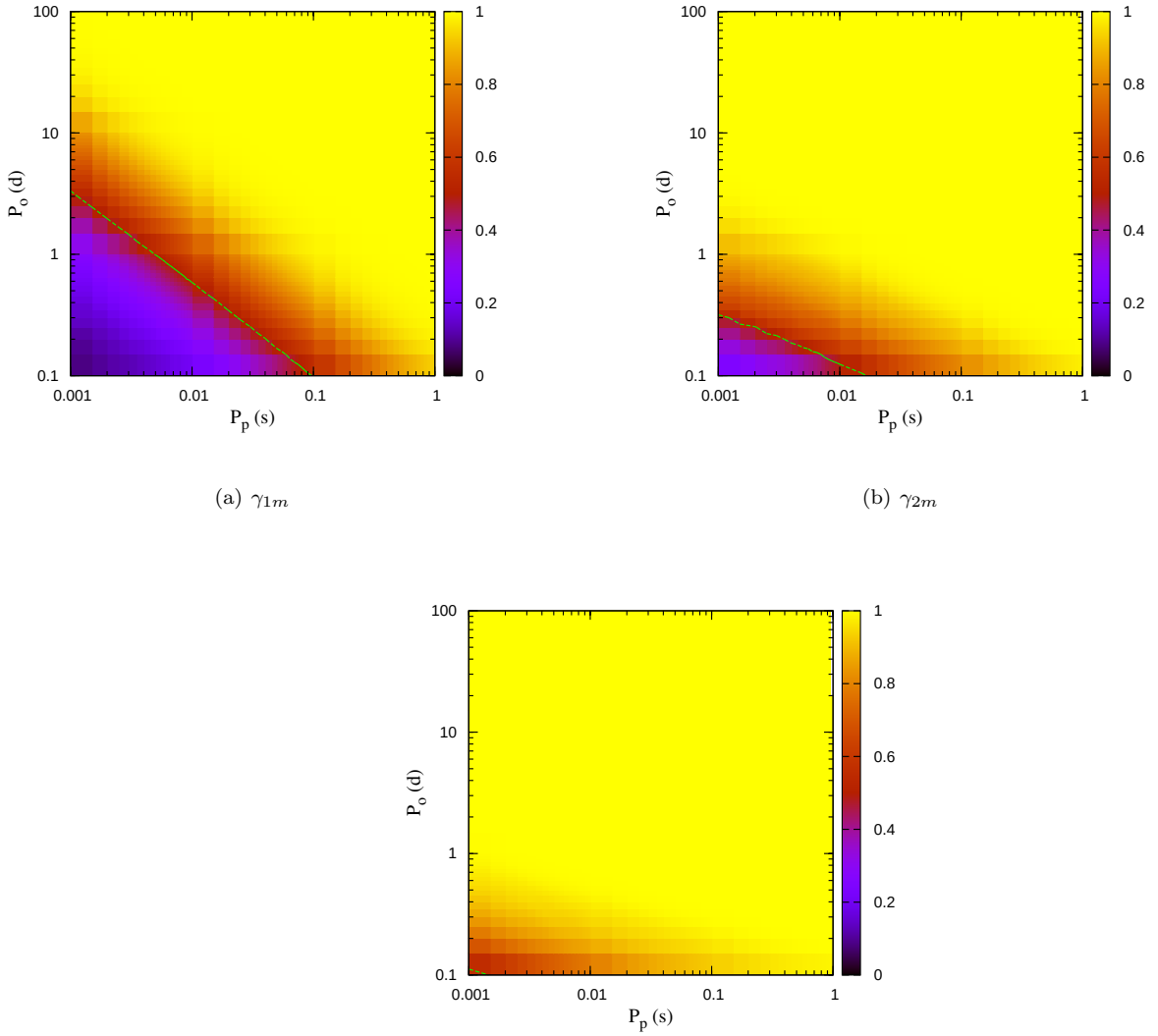

(a) γ_{1m}

(b) γ_{2m}

(c) γ_{3m}

Figure 16. Variation of γ_{1m}, γ_{2m}, and γ_{3m} with P_o and P_s for $M_p = 1.4\ M_\odot$, $M_c = 10.0\ M_\odot$, $\varpi = 30°$, $i = 60°$, $e = 0.5$, $m = 4$, and $T = 1000$ s.

Kramer, M., Stairs, I. H, 2008, ARA&A, 46, 541

Kramer, M., Stairs, I. H., Manchester, R. N., *et al.*, 2006, Science, 314, 97

Löhmer, O., Lewandowski, W., Wolszczan, A., Wielebinski, R., 2005, ApJ, 621, 388

Lorimer, D. R., "Binary and Millisecond Pulsars", Living Rev. Relativity 11, 2008, [Online Article]: cited on 13 August 2018, http://www.livingreviews.org/lrr-2008-8

Lorimer, D. R., Kramer, M., 2005, "Handbook of Pulsar Astronomy", Cambridge University Press

Lynch, R. S., Freire, P. C. C., Ransom, S. M., Jacoby, B. A., 2012, ApJ, 745, 109

Nice, David J., Splaver, E. M., Stairs, I. H., *et al.* , 2005, ApJ, 634, 1242

Nice, David J., Stairs, I. H., Kasian, L. E., 2007, AAS Meeting 211−102.06; Bulletin of the American Astronomical Society, 39, 918

Portegies Zwart, S., van den Heuvel, E. P. J., van Leeuwen, J., Nelemans, G., 2011, ApJ, 734, 55

Pfahl E., Podsiadlowski, P., Rappaport, S., 2005, ApJ, 628, 343

Radhakrishnan, V., Srinivasan, G., 1982, Current Science, 51, 1096

Ramachandran, R., Portegies Zwart, S. F.; 1998, Abstracts of the 19th Texas Symposium on Relativistic Astrophysics and

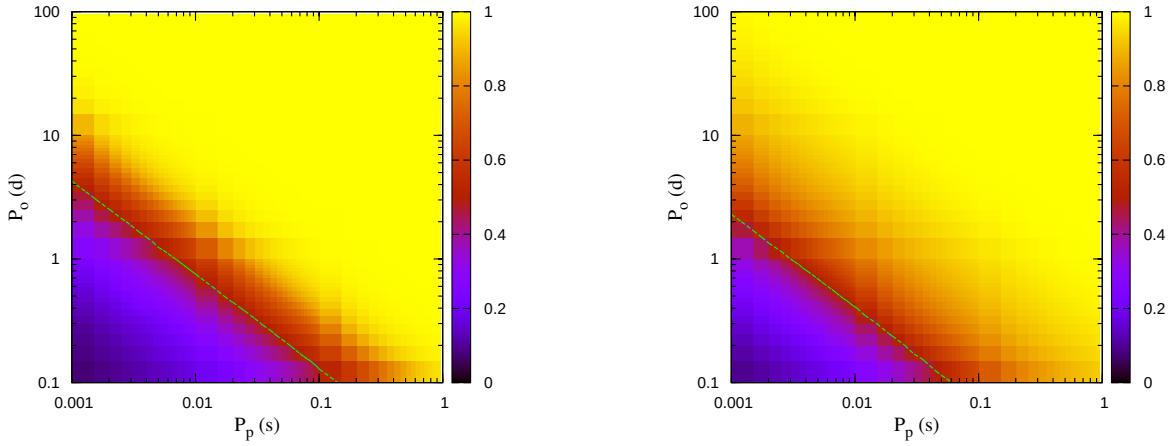

(a) $e = 0.1$ (b) $e = 0.8$

Figure 17. Variation of γ_{1m} with P_o and P_s for $M_p = 1.4\ M_\odot$, $M_c = 10.0\ M_\odot$, $\varpi = 30°$, $i = 60°$, $m = 4$, and $T = 1000$ s, for $e = 0.1$ and $e = 0.8$.

Cosmology, held in Paris, France, Dec. 14-18, 1998. Eds.: J. Paul, T. Montmerle, and E. Aubourg (CEA Saclay), meeting abstract; Portegies Zwart, S. F., private communication
Ransom, S. M., 2001, Ph. D Thesis, Harvard University
Ridley, J. P., Lorimer, D. R., 2010, MNRAS, 404, 1081
Smits, R., Kramer, M., Stappers, B., Lorimer, D. R., Cordes, J., Faulkner, A., 2009, A & A, 493, 1161
Splaver, E. M., Nice, D. J., Stairs, I. H., Lommen, A. N., Backer, D. C., 2005, ApJ, 620
Stairs, I. H., Thorsett, S. E., Taylor, J. H., Wolszczan, A., 2002, ApJ, 581, 501
Stairs, I. H., "Testing General Relativity with Pulsar Timing", Living Rev. Relativity 6, 2003, [Online Article]: cited on 13 August 2018, http://www.livingreviews.org/lrr-2003-5
Verbiest, J. P. W., Bailes, M., van Straten, W., *et al.*, 2008, ApJ, 679, 675
Verbiest, J. P. W., Bailes, M., Coles, W. A., 2009, MNRAS, 400, 951
Weisberg, J. M., Nice, D. J., Taylor, J. H., 2010, ApJ, 722, 1030